Journal of Inorganic Biochemistry 193 (2019) 173–179

Contents lists available at ScienceDirect

Journal of Inorganic Biochemistry

journal homepage: www.elsevier.com/locate/jinorgbio

Polyoxomolybdates as α-glucosidase inhibitors: Kinetic and molecular modeling studies

Guoxiang Chi[a], Yanfei Qi[b], Jian Li[a], Li Wang[a,*], Jingjing Hu[a]

[a] College of Food and Biological Engineering, Jimei University, Xiamen 361021, PR China
[b] School of Public Health, Jilin University, Changchun 130021, PR China

ARTICLE INFO

Keywords:
Polyoxomolybdates (POMs)
Enzyme kinetics
Molecular docking
α-Glucosidase inhibitors

ABSTRACT

Noninsulin dependent diabetes mellitus is a serious global disease that is treated by inhibiting α-glucosidase to reduce the glucose content in the blood. Several incompletely satisfactory therapeutic drugs are already on the market. In this report, we showed that polyoxomolybdates based on Keggin-type architecture are promising candidates. Kinetic studies indicate that $H_3PMo_{12}O_{40}$, $Na_4PMo_{11}VO_{40}$, $Na_6PMo_{11}FeO_{40}$ and $Na_7PMo_{11}CoO_{40}$ strongly inhibit α-glucosidase with IC_{50} values of 6.14 ± 0.38 μM, 52.33 ± 1.41 μM, 161.90 ± 7.68 μM and 103.10 ± 2.88 μM, respectively. Moreover, $H_3PMo_{12}O_{40}$, $Na_4PMo_{11}VO_{40}$, and $Na_7PMo_{11}CoO_{40}$ are reversible, competitive inhibitors with K_I values of 0.018 mM, 0.146 mM and 0.121 mM, respectively. $Na_6PMo_{11}FeO_{40}$ inhibited α-glucosidase in a reversible noncompetitive manner with K_I and K_{IS} of 0.312 mM and 0.412 mM, respectively. Molecular docking simulation suggested that $H_3PMo_{12}O_{40}$ binds into the substrate binding site in accordance with competitive inhibition behavior and offered, in addition, an initial insight into the polypeptide-inhibitor interactions. This work presents a promising new perspective for designing effective α-glucosidase inhibitors and further demonstrates the enormous potential of polyoxomolybdates as enzyme inhibitors.

1. Introduction

Type 2 diabetes, the main type of diabetes mellitus (DM), is currently recognized as a serious global health problem. Type 2 diabetes is a type of noninsulin-dependent diabetes caused by insulin deficiency or insulin resistance [1,2]. α-Glucosidase is a carbohydrate hydrolase, and the inhibition of its activity may delay the digestion of carbohydrates and thereby reduce the amount of glucose absorbed into the blood [3,4]. Thus, α-glucosidase is considered to be an important target for the treatment of noninsulin-dependent diabetes mellitus and for the design of many α-glucosidase inhibitors [5]. At present, the research of domestic and foreign scholars on α-glucosidase inhibitors mainly focuses on natural extracts and organic compounds. Jang et al. [6] reported that scopoletin might contribute to relieving postprandial hyperglycemia through the inhibition of carbohydrate digestive enzymes. Ding et al. [7] designed and synthesized a series of novel oxazolxanthones that showed good inhibition of α-glucosidase by studies of enzyme kinetics and molecular docking. However, few inorganic agents capable of inhibiting α-glucosidase have been reported. In addition, high efficiency, low cytotoxicity and low cost are the key factors to be considered in the design of α-glucosidase inhibitors. Herein, current therapeutic drugs (acarbose, voglibose and miglitol) have been used clinically for many years, but the clinical application of these compounds has always been limited by their high cost and side effects [8]. Therefore, designing novel, safe and effective α-glucosidase inhibitors is an attractive goal in the field of medicinal chemistry.

Polyoxomolybdates (abbreviated as POMs), due to their incomparable structural diversity and novel functional properties, have been widely studied in various fields (Table S1), such as catalysis [9–11], medicine [12,13], material science [14,15], photoelectrochemistry [16,17] and self-assembled nanozymes [13,18]. Especially in the field of medicine, POMs are promising candidates for drug-carrier approaches on the path to the identification of new composite drugs because they have long been known for their multifaceted bioactivities that encompass anticancer, anti-tumor, antiviral and antibacterial effects [19–23]. Furthermore, the inhibitory effect of POMs on various enzyme activities has become a hotspot for research and the development of safe, nontoxic and high-efficiency enzyme inhibitors for POM properties has escalated in recent years. Many studies have demonstrated that POMs possess significant inhibitory effects on the activities of nucleotidases, phosphatases, kinases, sulfotransferases, sialyltransferases, acetylases, nucleases and proteases [24,25]. Gumerova et al. [26] analyzed and compared the inhibitory effects of nine different polyoxotungstates (POTs) on two P-type ATPases, and the results

* Corresponding author.
E-mail address: wanglimerry@jmu.edu.cn (L. Wang).

https://doi.org/10.1016/j.jinorgbio.2019.02.001
Received 5 October 2018; Received in revised form 17 January 2019; Accepted 1 February 2019
Available online 08 February 2019
0162-0134/

reveal the high potential of some POTs to act as P-type ATPase inhibitors, with $K_9(C_2H_8N)_5[H_{10}Se_2W_{29}O_{103}]$ showing high selectivity towards Ca^{2+}-ATPase. Lee et al. [27] evaluated the inhibitory potency of a series of POMs as well as chalcogenide hexarhenium cluster complexes against a broad range of ecto-nucleotidases, and the $[Co_4(H_2O)_2(PW_9O_{34})_2]^{10-}$(5, PSB -POM 142) was discovered to be the most potent inhibitor of human NTPDase1.

Moreover, in comparison to mononuclear complexes, POMs have been markedly under-studied in the context of diabetes [23,28]. Ilyas et al. [29] evaluated the inhibitory effects of different polytungstates on glucosidases (α- and β) in vitro and in vivo, and the research showed that $Na_{20}[P_6W_{18}O_{79}]\cdot 37H_2O$ (Na-P_6W_{18}) was the most potent inhibitor of α-glucosidase (IC_{50} = 1.33 ± 0.41 μM). Although some functionalized POMs have been used as inhibitors of α-glucosidase, their molecular mechanism of action is largely unknown. As a result of insightful studies on POMs for α-glucosidase, compounds with improved pharmacological properties might be developed for the treatment of diabetes. Furthermore, Keggin-type POMs and their derivatives exhibit better biological activities and lower cytotoxicities [30–32] and may become potentially effective enzyme inhibitors.

However, it is unclear whether the parent and transition metal substitution in Keggin-type phosphomolybdic acid will reveal the best effects on α-glucosidase. Therefore, the Keggin-type $H_3PMo_{12}O_{40}$ (abbreviated as PMo_{12}) and three transition metal-substituted POMs ($Na_4PMo_{11}VO_{40}$, $Na_6PMo_{11}FeO_{40}$ and $Na_7PMo_{11}CoO_{40}$, abbreviated as $PMo_{11}V$, $PMo_{11}Fe$ and $PMo_{11}Co$) were synthesized and characterized. The inhibitory effect of these four compounds on α-glucosidase was studied by enzyme kinetics. In addition, to further study the binding forms and interactions of α-glucosidase and Keggin-type phosphomolybdic acid, the inhibitor PMo_{12} was used as a ligand for molecular docking simulation in the following studies. This work provided an enlightened strategy for expanding the applications of Keggin-type phosphomolybdic acid and for designing new and effective α-glucosidase inhibitors.

2. Materials and methods

2.1. Reagents

PMo_{12}, $PMo_{11}V$, $PMo_{11}Fe$ and $PMo_{11}Co$ were synthesized as previously described [33,34], with slight modifications. Briefly, 0.025 mol the reagent (NH_4VO_3, $FeCl_3$ and $CoCl_2\cdot 6H_2O$), 1.72 mL H_3PO_4 (85%) and 0.29 mol $Na_2MoO_4\cdot 2H_2O$ were dissolved in 400 mL ultrapure water. After 7 h of circumfluence heating, the solution was cooled to room temperature, acidified with 75 mL hydrochloric acid and extracted with ether. Next, the lower solution was collected, and the powder was obtained by recrystallization several days later. The structure of the powder was then characterized by IR (Jasco FT/IR-480) and UV/*Vis* (Cary-50) spectroscopy. α-Glucosidase of *S. cerevisiae* (EC 3.2.1.20), *p*-nitrophenyl-α-D-glucopyranoside (*p*NPG), *p*-nitrophenol (*p*NP) and dimethyl sulfoxide (DMSO) were purchased from Sigma-Aldrich Chemical Co. (USA). All other reagents were locally sourced and of analytical grade, and ultra-pure water was used throughout.

2.2. Experimental procedures

2.2.1. Enzyme kinetics analysis

The α-glucosidase activity assay was performed as previously described [35], with slight modifications. *p*NPG was used as a substrate to generate a yellow product (*p*NP) with catalysis by α-glucosidase in this experiment, and the OD value after the reaction of the system was monitored by microplate reader (Synergy H1) at a wavelength of 405 nm. Briefly, the reaction system was sequentially supplemented with 133 μL of 0.1 M phosphate buffer (Na_2HPO_4-NaH_2PO_4 buffer, pH 6.8), 7 μL of different concentrations of inhibitors completely dissolved in DMSO solution (the final concentration of DMSO in the test solution was 5%), and 10 μL of α-glucosidase solution that was added immediately. Next, the mixture was incubated at 37.0 °C for 10 min, and 20 μL of the substrate (*p*NPG) preheated at 37.0 °C for 10 min was added to the mixture. The reaction was carried out at 37.0 °C for 20 min, and then the reaction was terminated by the addition of an equal volume of Na_2CO_3 solution (1 M). The OD value of the 200 μL reaction solution was monitored in a 96-well plate by using the microplate reader at 405 nm.

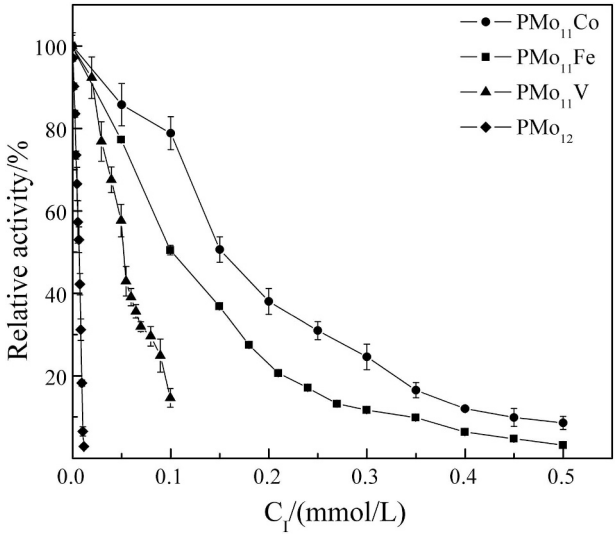

Fig. 1. Inhibitory effect of Keggin-type PMo_{12} and the three transition metal-substituted polyoxomolybdates on the activity of α-glucosidase. Error bars indicate ± s.d.

Under the conditions of constant substrate concentration and enzyme concentration, the inhibitory effect of the inhibitor on α-glucosidase was determined by changing the concentration of the inhibitor added. In addition, the inhibition mechanism of the inhibitor on α-glucosidase was determined, under conditions of constant substrate concentration, by changing the concentration of the added enzyme and the concentration of the inhibitor. Moreover, the inhibition type of the inhibitor was assayed by the Lineweaver-Burk plot (double-reciprocal plot), and the inhibition constants (K_I or K_{IS}) were obtained by the second plots of the apparent K_m/V_m or $1/V_m$ versus the concentration of the inhibitor. DMSO without any inhibitor was used as a control [36].

2.2.2. Molecular docking study

To predict the binding mode of the synthesized PMo_{12} with α-glucosidase, a molecular docking study was carried out using the MOE (Molecular Operating Environment) software package. The three-dimensional structures of the synthesized PMo_{12} were generated via the builder tool in the MOE. The generated compound was 3D protonated and energy minimized using the default parameters of the MOE (gradient: 0.05, Force Field: MMFF94X). The compound was then saved into an .mdb file for further evaluation [37,38].

The α-glucosidase of *S. cerevisiae* has been widely used in the screening of bioactive compounds targeting α-glucosidase, but the 3D structure of the α-glucosidase of *S. cerevisiae* has not yet been solved. The template structure and crystal structure of isomaltase from *S. cerevisiae* (PDB 3AJ7) share 82% homology with the *S. cerevisiae* α-glucosidase, which is generally considered as an excellent value for the selection of template [39]. Moreover, the primary sequence of *S. cerevisiae* α-glucosidase was retrieved from UniProt (Accession code P53341) [40]. Using the MAL32 target sequence and the crystal structure of isomaltase from *S. cerevisiae* (PDB 3AJ7) as a template, we constructed the α-glucosidase homology model in SWISS-MODEL, and the stereochemical quality of the model was assessed using the Ramachandran plot. The evaluation of the backbone Psi and Phi dihedral

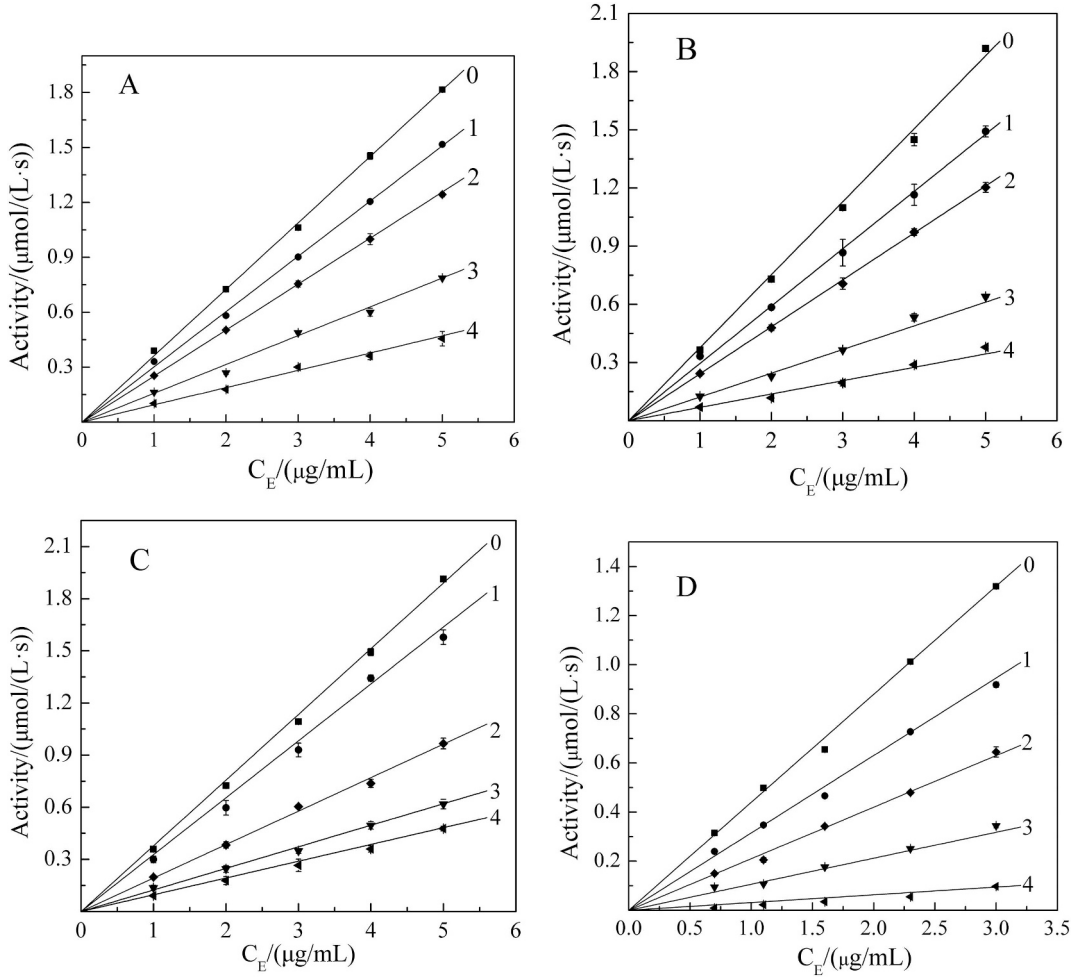

Fig. 2. Inhibitory mechanism of Keggin-type PMo_{12} and the three transition metal-substituted polyoxomolybdates ($PMo_{11}V$, $PMo_{11}Fe$ and $PMo_{11}Co$) on the activity of α-glucosidase. The concentrations of PMo_{12} for curves 0–4 of Fig. 2A were 0, 0.01, 0.02, 0.025 and 0.03 mmol L^{-1}, respectively. The concentrations of $PMo_{11}V$ for curves 0–4 of Fig. 2B were 0, 0.02, 0.03, 0.05 and 0.08 mmol L^{-1}, respectively. The concentrations of $PMo_{11}Fe$ for curves 0–4 of Fig. 2C were 0, 0.05, 0.1, 0.15 and 0.2 mmol L^{-1}, respectively. The concentrations of $PMo_{11}Co$ for curves 0–4 of Fig. 2D were 0, 0.025, 0.05, 0.13 and 0.2 mmol L^{-1}, respectively. Error bars indicate ± s.d.

angles for the α-glucosidase model revealed that 95% of the residues lie in the favored region and that only one residue (0.3%) exhibited a disallowed conformation (Phe303). The results of the Ramachandran plot reflect the accuracy of our modeled structure used in the docking protocol. Thus, we used our reported 3D homology model of isomaltase of *S. cerevisiae*.

For molecular docking simulation, we used the Triangle Matcher method to place small molecules, and the London dG function scored the docking results. The concrete parameters of the MOE used were: Placement: Triangle Matcher, Rescoring 1: London dG, Refinement: Forcefield, Rescoring 2: London dG. For each ligand, 10 conformations were allowed to be formed and the top ranked conformations were selected on the basis of docking score for further analysis. Furthermore, the docking score is the binding free energy calculated by the London dG scoring function, which is the score of the last stage showing the overall stability of the predicted complex. For all scoring functions, lower scores indicate more favorable poses. The unit for all scoring functions is kcal/mol [37].

2.2.3. Statistical analysis

The experimental data acquisitions were repeated five times under parallel determination by using SPSS version 17.0 and GraphPad Prism version 7.0 for analysis. Experimental drawings were completed using Origin 8.0 professional software. Error bars indicate ± s.d.

3. Results and discussion

3.1. Spectroscopic characterization

Table S2 lists the IR spectra data of compounds PMo_{12}, $PMo_{11}V$, $PMo_{11}Fe$ and $PMo_{11}Co$. As shown in Table S2, all four compounds exhibit the characteristic bands of the Keggin-type structure, and there are four characteristic peaks (P-O_a anti-symmetric stretching vibration peak, Mo-O_d anti-symmetric stretching vibration peak, Mo-O_b-Mo anti-symmetric stretching vibration peak and Mo-O_c-Mo anti-symmetric stretching vibration peak) in the range of 700–1100 cm^{-1}. These results were consistent with data from the literature [33,34] and indicated that the synthesized compound was a Keggin-type compound.

Table S3 lists the UV/*Vis* spectra data of the compounds PMo_{12}, $PMo_{11}V$, $PMo_{11}Fe$ and $PMo_{11}Co$. As shown in Table S3, the four compounds exhibit characteristic absorption bands approximately 200 nm and 260 nm, which correspond to the charge transfer transitions of O_d-Mo and O_b/O_c-Mo, respectively. The above results suggested that the synthesized compounds all possess a Keggin-type heteropoly acid structure, which is consistent with the results of reference [34]. The peak positions of the compounds in the table are shifted, which may be

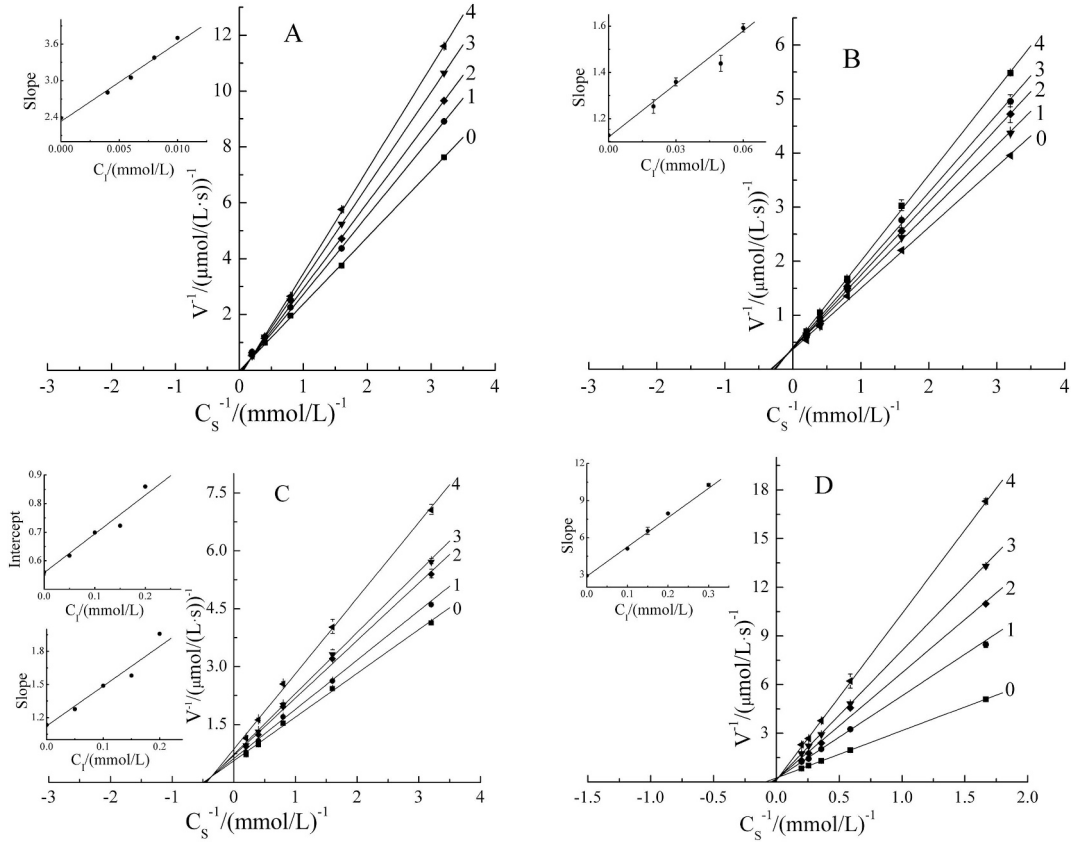

Fig. 3. Inhibitory type of Keggin-type PMo_{12} and the three transition metal-substituted polyoxomolybdates ($PMo_{11}V$, $PMo_{11}Fe$ and $PMo_{11}Co$) on the activity of α-glucosidase. The inset of Fig. 3ABD represents the secondary plot of the slope versus the concentrations of PMo_{12}, $PMo_{11}V$ and $PMo_{11}Co$ in order to determine the inhibition constant (K_I). The inset of Fig. 3C represents the secondary plot of the slope and intercept, respectively, versus the concentrations of $PMo_{11}Fe$ to determine the inhibition constants (K_I and K_{IS}). The concentrations of PMo_{12} for curves 0–4 of Fig. 3A were 0, 0.004, 0.006, 0.008 and 0.01 mmol L^{-1}, respectively. The concentrations of $PMo_{11}V$ for curves 0–4 of Fig. 3B were 0, 0.02, 0.03, 0.05 and 0.06 mmol L^{-1}, respectively. The concentrations of $PMo_{11}Fe$ for curves 0–4 of Fig. 3C were 0, 0.05, 0.1, 0.15 and 0.2 mmol L^{-1}, respectively. The concentrations of $PMo_{11}Co$ for curves 0–4 of Fig. 3D were 0, 0.1, 0.15, 0.2 and 0.3 mmol L^{-1}, respectively. Error bars indicate ± s.d.

due to the substitution of transition metals.

3.2. The inhibitory effects of compounds against α-glucosidase

Inhibition studies on α-glucosidase with the compounds PMo_{12}, $PMo_{11}V$, $PMo_{11}Fe$ and $PMo_{11}Co$ (Fig. S1), applying pNPG as substrate, revealed a significant decrease in the enzymatic activity with increased Keggin-type POMs concentrations (Fig. 1). The concentrations of PMo_{12}, $PMo_{11}V$, $PMo_{11}Fe$, and $PMo_{11}Co$ when the α-glucosidase activity was decreased by 50% (IC_{50}) were 6.41 ± 0.38 μM, 52.33 ± 1.41 μM, 161.90 ± 7.68 μM and 103.10 ± 2.88 μM, respectively. Comparing the IC_{50} of each inhibitor, the above results suggested that the phosphomolybdic acid parent compound (PMo_{12}) exerts a better inhibitory effect on α-glucosidase than does the transition metal-substituted phosphomolybdic acid, in which the transition metal substitution may weaken the inhibition of α-glucosidase. In addition, the results also indicated that $PMo_{11}V$ exerts a better inhibitory effect on α-glucosidase than those of $PMo_{11}Fe$ and $PMo_{11}Co$. At the same time, compared with the IC_{50} of standard commercial acarbose (IC_{50} = 750 ± 1.5 μM) [41], the inhibition potency of the parent PMo_{12} was approximately 117 times higher than that of standard acarbose; therefore, the compounds synthesized in our laboratory demonstrate more significant inhibitory effects on α-glucosidase.

Furthermore, with different concentrations of PMo_{12}, $PMo_{11}V$, $PMo_{11}Fe$ and $PMo_{11}Co$ as inhibitors, 5 mM PNPG solution was used as substrate to study the inhibitory mechanism of the inhibitors on α-glucosidase activity. The results are shown in Fig. 2. In the reaction system, the plots of the remaining enzyme activity versus the concentrations of the enzyme produced several adjacent straight lines, which all passed through the origin. Next, a linear decrease with increasing concentrations of inhibitors indicated that the inhibition mechanisms of these four inhibitors on α-glucosidase were reversible [42]. Thus, these four inhibitors reversibly combined with the enzyme in the form of noncovalent bonds, which resulted in decreased enzyme activity.

In addition, in the phosphate buffer reaction system with a fixed enzyme concentration of 5 U/mL, the inhibition type of the inhibitor on the α-glucosidase activity was determined using the Lineweaver-Burk (double-reciprocal) plots of the reciprocal of the reaction rate versus the reciprocal of the substrate concentration. The inhibitory constant (K_I or K_{IS}) of the inhibitors was further calculated through secondary mapping, and the results are shown in Fig. 3. As shown in Fig. 3(ABD), the graph of 1/v versus 1/[s] represented a set of straight lines which all intersected at or extremely close to the Y-axis. Next, the linear slope increased gradually as the concentrations of the PMo_{12}, $PMo_{11}V$ and $PMo_{11}Co$ inhibitors increased, while the vertical axis intercept remained unchanged, which suggested that the inhibitory types of these three inhibitors were competitive [42]. As shown in Fig. 3(C), the graph of 1/v versus 1/[s] was a set of straight lines which all intersected at the X-axis. The change in the $PMo_{11}Fe$ concentration resulted in changes in the linear slope and the vertical intercept, which suggested that the inhibition type of $PMo_{11}Fe$ was noncompetitive [42]. Moreover, the inhibitory constants K_I of the inhibitors (PMo_{12}, $PMo_{11}V$, $PMo_{11}Fe$ and $PMo_{11}Co$) were calculated by further plotting the linear slopes versus

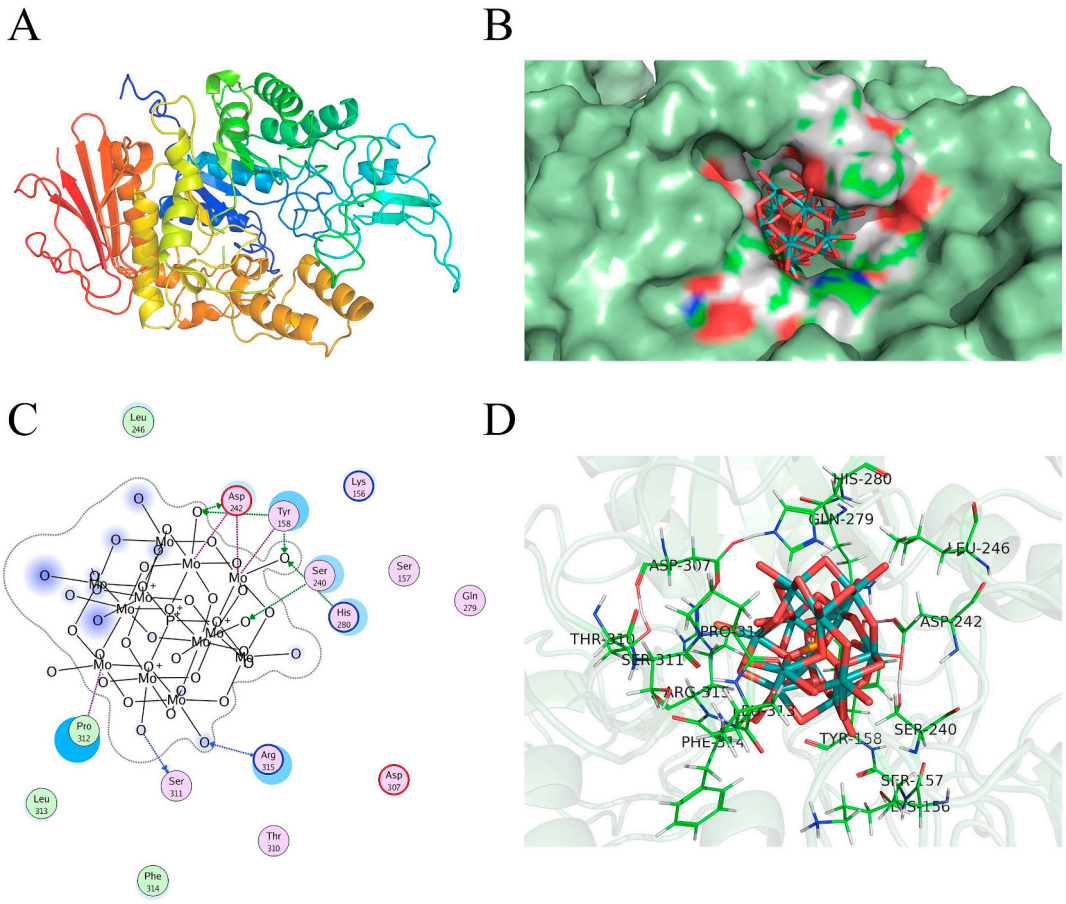

Fig. 4. Docking conformations of compound PMo_{12} in α-glucosidase enzyme. (A) 3D crystal structure of *S. cerevisiae* isomaltase (PDB 3AJ7). (B) Compound PMo_{12} in the active site of α-glucosidase. (C) Two-dimensional ligand interaction map of compound PMo_{12} docked into the binding site of α-glucosidase. (D) Three-dimensional complex interaction of α-glucosidase and the PMo_{12} compound.

the inhibitor concentrations of 0.018 mM, 0.146 mM, 0.312 mM and 0.121 mM, respectively. By further plotting the vertical intercept against the concentration of the inhibitor, the inhibition constant K_{IS} of $PMo_{11}Fe$ was calculated to be 0.412 mM.

3.3. Analysis of molecular docking results

Because the 3D structure of α-glucosidase of *S. cerevisiae* has not yet been solved, we used our reported 3D homology model of isomaltase of *S. cerevisiae* (PDB 3AJ7) as a molecular docking model, as shown in Fig. 4(A). To study the interactions of the synthesized compounds in the active site of α-glucosidase and their related inhibitory activities, docking studies were performed using the most potent compound PMo_{12} as a ligand. The molecular binding model by molecular docking is shown in Fig. 4(BCD). The conformation of the ligand is the lowest conformation of free energy docking with α-glucosidase. Next, the compound PMo_{12} in the active site of α-glucosidase is shown in Fig. 4(B). In addition, Fig. 4(C) shows the hydrogen bonding interaction and the van der Waals interactions generated by the MOE between the surrounding important amino acid residues and the ligand small molecules. As shown in Fig. 4(C), the amino acid residues surrounding the compound are represented by pink and green circles. PMo_{12} accurately fits into the deep pocket of the active site and is largely surrounded by the polypeptide. After docking scoring, the docking score is determined as −14.7951 kcal/mol. The smaller the numerical value is, the better is the ability of the compound to bind to the biomacromolecule. In general, an inhibitor of approximately −7 kcal/mol is effective, and this compound reaches −14.7951 kcal/mol, indicating that the compound has a considerable inhibitory effect on α-glucosidase [4].

To vividly represent the binding forms and interactions of α-glucosidase and the compound PMo_{12}, a visual three-dimensional simulation map was created using Pymol software, which is shown in Fig. 4(D). These two visualization software packages complement each other to show a more comprehensive view of interactions between the binding site amino acid residues and ligand small molecule in the system.

Furthermore, as shown in Fig. 4(CD), the compound PMo_{12} initiated 7 hydrogen bonding interactions with the amino acid residues (Tyr158, Ser240, Asp242, His280, Ser311 and Arg315) in the active region. Among them, the five O atoms in the PMo_{12} skeleton can form seven hydrogen bonds with the H atoms in the amino acid residues. Hydrogen bonding is a common form of bonding between drug molecules and receptor biomacromolecules which can increase the activity of drugs. Moreover, binding to the enzyme in the form of hydrogen bonds, the compound also forms van der Waals interactions with the amino acid residues (Lys156, Ser157, Leu246, Gln279, Asp307, Thr310, Pro312, Leu313 and Phe314) around the active region. More van der Waals interactions may cause higher activity of the compound (increased hydrophobicity will be beneficial to increase the inhibition activity of the compound). According to the above results, the compound does not bind to the enzyme active groups in a relatively firm covalent bond, but in the form of hydrogen bonding and van der Waals interactions. Therefore, the catalytic group of the enzyme is generally not destroyed, and the enzyme is not inactivated, which proves that the compound is a reversible inhibitor.

In addition, in the analysis of docking interaction residues, there are 11 polar amino acid residues (Lys156, Ser157, Tyr158, Ser240, Asp242, Gln279, His280, Asp307, Thr310, Ser311 and Arg315) around the

active binding site of the enzyme. It can be found that the polar properties of the small molecules are important for enzyme interactions. In general, when a ligand binds to the active site of the receptor, the active site of the ligand forms a hydrogen bond with the polar amino acid residue in the active site of the receptor, and the hydrophobic portion of the ligand can produce a hydrophobic effect with the nonpolar amino acid residues within the active site of the receptor.

4. Conclusions

In summary, PMo_{12} and three transition metal-substituted Keggin-type phosphomolybdic acids ($PMo_{11}V$, $PMo_{11}Fe$ and $PMo_{11}Co$) could effectively inhibit α-glucosidase activity by enzyme kinetics, and the inhibitory effect of PMo_{12} was approximately 117 times higher than that of standard acarbose [41]. Moreover, combining the inhibition mechanism and the type of inhibition, we found that the inhibitors PMo_{12}, $PMo_{11}V$ and $PMo_{11}Co$ showed reversible competitive inhibition of α-glucosidase, while $PMo_{11}Fe$ showed reversible noncompetitive inhibition of α-glucosidase. In addition, molecular modeling experiments showed that the inhibitor PMo_{12} mainly binds to the amino acid molecules of the active site in the α-glucosidase molecule through hydrogen bonding and van der Waals interaction. Therefore, the enzyme is not inactivated and the inhibition mechanism is reversible. According to the obtained experimental results above, we further demonstrated the results of enzyme kinetic experiments and further expound upon the mechanisms of action at the molecular level. This work provided an ideal strategy for designing α-glucosidase inhibitors with high efficiency, low cytotoxicity [32,43] and low cost. Due to the complex mechanisms of action of Keggin-type POMs with respect to α-glucosidase, the need for further research is emphasized. Through future experiments, we will determine the active site and substrate-binding mode of α-glucosidase by using site-directed mutagenesis and comparative modeling methods, and we will expand our investigation by analogous inhibition studies with the human α-glucosidase and the model enzyme isomaltase. In a sense, our work advances our understanding of the design and synthesis of Keggin-type phosphomolybdic acids as multifunctional therapeutic agents against type 2 diabetes.

Supplementary data to this article can be found online at https://doi.org/10.1016/j.jinorgbio.2019.02.001.

Acknowledgements

This work was supported by the National Natural Science Foundation of China (Grant No. 21871110).

References

[1] S.H. Ley, A.V. Ardisson Korat, Q. Sun, D.K. Tobias, C. Zhang, L. Qi, W.C. Willett, J.E. Manson, F.B. Hu, Contribution of the Nurses' Health Studies to uncovering risk factors for type 2 diabetes: diet, lifestyle, biomarkers, and genetics, Am. J. Public Health 106 (9) (2016) 1624–1630, https://doi.org/10.2105/AJPH.2016.303314.

[2] A. Migdal, M. Abrahamson, A. Peters, N. Vint, Approaches to rapid acting insulin intensification in patients with type 2 diabetes mellitus not achieving glycemic targets, Ann. Med. (2018) 1–27, https://doi.org/10.1080/07853890.2018.1493216.

[3] M. Adib, F. Peytam, M. Rahmanian-Jazi, S. Mahernia, H.R. Bijanzadeh, M. Jahani, M. Mohammadi-Khanaposhtani, S. Imanparast, M.A. Faramarzi, M. Mahdavi, B. Larijani, New 6-amino-pyrido [2,3-d] pyrimidine-2, 4-diones as novel agents to treat type 2 diabetes: a simple and efficient synthesis, α-glucosidase inhibition, molecular modeling and kinetic study, Eur. J. Med. Chem. 155 (2018) 353–363, https://doi.org/10.1016/j.ejmech.2018.05.046.

[4] M. Zafar, H. Khan, A. Rauf, A. Khan, M.A. Lodhi, *In silico* study of alkaloids as α-glucosidase inhibitors: hope for the discovery of effective lead compounds, Front. Endocrinol. 7 (2016) 1–17, https://doi.org/10.3389/fendo.2016.00153.

[5] D.N. Olennikov, N.K. Chirikova, N.I. Kashchenko, V.M. Nikolaev, S.W. Kim, C. Vennos, Bioactive phenolics of the genus *Artemisia* (asteraceae): HPLC-DAD-ESI-TQ-MS/MS profile of the Siberian species and their inhibitory potential against α-amylase and α-glucosidase, Front. Pharmacol. 9 (2018) 756–783, https://doi.org/10.3389/fphar.2018.00756.

[6] J.H. Jang, J.E. Park, J.S. Han, Scopoletin inhibits α-glucosidase *in vitro* and alleviates postprandial hyperglycemia in mice with diabetes, Eur. J. Pharmacol. 834 (2018) 152–156, https://doi.org/10.1016/j.ejphar.2018.07.032.

[7] S.M. Ding, T. Lan, G.J. Ye, J.J. Huang, Y. Hu, Y.R. Zhu, B. Wang, Novel oxazolxanthone derivatives as a new type of α-glucosidase inhibitor: synthesis, activities, inhibitory modes and synergetic effect, Bioorg. Med. Chem. 26 (12) (2018) 3370–3378, https://doi.org/10.1016/j.bmc.2018.05.008.

[8] M. Toeller, α-Glucosidase inhibitors in diabetes: efficacy in NIDDM subjects, Eur. J. Clin. Investig. 24 (S3) (1994) 31–35, https://doi.org/10.1111/j.1365-2362.1994.tb02253.x.

[9] F. Zhang, Y. Jin, J. Shi, Y. Zhong, W. Zhu, M.S. El-Shall, Polyoxometalates confined in the mesoporous cages of metal-organic framework MIL-100 (Fe): efficient heterogeneous catalysts for esterification and acetalization reactions, Chem. Eng. J. 269 (2015) 236–244, https://doi.org/10.1016/j.cej.2015.01.092.

[10] S.J. Folkman, J. Soriano-Lopez, J.R. Galán-Mascarós, R.G. Finke, Electrochemically driven water-oxidation catalysis beginning with six exemplary cobalt polyoxometalates: is it molecular, homogeneous catalysis or electrode-bound, heterogeneous CoO_x catalysis? J. Am. Chem. Soc. 140 (38) (2018) 12040–12055, https://doi.org/10.1021/jacs.8b06303.

[11] Y. Liu, S. Liu, D. He, N. Li, Y. Ji, Z. Zheng, F. Luo, S. Liu, Z. Shi, C. Hu, Crystal facets make a profound difference in polyoxometalate-containing metal-organic frameworks as catalysts for biodiesel production, J. Am. Chem. Soc. 137 (39) (2015) 12697–12703, https://doi.org/10.1021/jacs.5b08273.

[12] M. Ma, N. Gao, Y. Sun, X. Du, J. Ren, X. Qu, Redox-activated near-infrared-responsive polyoxometalates used for photothermal treatment of Alzheimer's disease, Adv. Healthc. Mater. (2018) e1800320, , https://doi.org/10.1002/adhm.201800320.

[13] N. Gao, K. Dong, A. Zhao, H. Sun, Y. Wang, J. Ren, X. Qu, Polyoxometalate-based nanozyme: design of a multifunctional enzyme for multi-faceted treatment of Alzheimer's disease, Nano Res. 9 (4) (2016) 1079–1090, https://doi.org/10.1007/s12274-016-1000-6.

[14] C.T. Buru, A.E. Platero-Prats, D.G. Chica, M.G. Kanatzidis, K.W. Chapman, O.K. Farha, Thermally induced migration of a polyoxometalate within a metal-organic framework and its catalytic effects, J. Mater. Chem. A 6 (17) (2018) 7389–7394, https://doi.org/10.1039/C8TA02562B.

[15] S. Taleghani, M. Mirzaei, H. Eshtiagh-Hosseini, A. Frontera, Tuning the topology of hybrid inorganic-organic materials based on the study of flexible ligands and negative charge of polyoxometalates: a crystal engineering perspective, Coord. Chem. Rev. 309 (2016) 84–106, https://doi.org/10.1016/j.ccr.2015.10.004.

[16] C. Allain, D. Schaming, N. Karakostas, M. Erard, J.P. Gisselbrecht, S. Sorgues, I. Lampre, L. Ruhlmann, B. Hasenknopf, Synthesis, electrochemical and photophysical properties of covalently linked porphyrin-polyoxometalates, Dalton Trans. 42 (8) (2013) 2745–2754, https://doi.org/10.1039/C2DT31415K.

[17] X.J. Kong, Z. Lin, Z.M. Zhang, T. Zhang, W. Lin, Hierarchical integration of photosensitizing metal-organic frameworks and nickel-containing polyoxometalates for efficient visible-light-driven hydrogen evolution, Angew. Chem. Int. Ed. 55 (22) (2016) 6411–6416, https://doi.org/10.1002/ange.201600431.

[18] Y. Guan, M. Li, K. Dong, N. Gao, J. Ren, Y. Zheng, X. Qu, Ceria/POMs hybrid nanoparticles as a mimicking metallopeptidase for treatment of neurotoxicity of amyloid-β peptide, Biomaterials 98 (2016) 92–102, https://doi.org/10.1016/j.biomaterials.2016.05.005.

[19] N. Gao, H. Sun, K. Dong, J. Ren, T. Duan, C. Xu, X. Qu, Transition-metal-substituted polyoxometalate derivatives as functional anti-amyloid agents for Alzheimer's disease, Nat. Commun. 5 (2014) 1–19, https://doi.org/10.1038/ncomms4422.

[20] A. Bijelic, M. Aureliano, A. Rompel, Polyoxometalates as potential next-generation metallodrugs in the combat against cancer, Angew. Chem. Int. Ed. 57 (2018) 2–22, https://doi.org/10.1002/anie.201803868.

[21] A. Bijelic, M. Aureliano, A. Rompel, The antibacterial activity of polyoxometalates: structures, antibiotic effects and future perspectives, Chem. Commun. 54 (10) (2018) 1153–1169, https://doi.org/10.1039/c7cc07549a.

[22] J. Liu, W.J. Mei, A.W. Xu, C.P. Tan, S. Shi, L.N. Ji, Synthesis, characterization and antiviral activity against influenza virus of a series of novel manganese-substituted rare earth borotungstates heteropolyoxometalates, Antivir. Res. 62 (1) (2004) 65–71, https://doi.org/10.1016/j.antiviral.2003.12.004.

[23] B. Hasenknopf, Polyoxometalates: introduction to a class of inorganic compounds and their biomedical applications, Front. Biosci. 10 (1–3) (2005) 275–287, https://doi.org/10.2741/1527.

[24] H. Stephan, M. Kubeil, F. Emmerling, C.E. Müller, Polyoxometalates as versatile enzyme inhibitors, Eur. J. Inorg. Chem. 2013 (10 − 11) (2013) 1585–1594, https://doi.org/10.1002/ejic.201201224.

[25] A. Seko, T. Yamase, K. Yamashita, Polyoxometalates as effective inhibitors for sialyl-and sulfotransferases, J. Inorg. Biochem. 103 (7) (2009) 1061–1066, https://doi.org/10.1016/j.jinorgbio.2009.05.002.

[26] N. Gumerova, L. Krivosudský, G. Fraqueza, J. Breibeck, E. Al-Sayed, E. Tanuhadi, A. Bijelic, J. Fuentes, M. Aureliano, A. Rompel, The P-type ATPase inhibiting potential of polyoxotungstates, Metallomics 10 (2018) 287–295, https://doi.org/10.1039/c7mt00279c.

[27] S.Y. Lee, A. Fiene, W. Li, T. Hanck, K.A. Brylev, V.E. Fedorov, J. Lecka, A. Haider, H. Pietzsch, H. Zimmermann, J. Sévigny, U. Kortz, H. Stephan, C.E. Müller, Polyoxometalates-potent and selective ecto-nucleotidase inhibitors, Biochem. Pharmacol. 93 (2) (2015) 171–181, https://doi.org/10.1016/j.bcp.2014.11.002.

[28] W. Liu, R. Al-Oweini, K. Meadows, B.S. Bassil, Z. Lin, J.H. Christian, N.S. Dalal, A.M. Bossoh, I.M. Mbomekallé, P. de Oliveira, J. Iqbal, Cr^{III}-substituted heteropoly-16-tungstates $[Cr_2^{III}(B\text{-}\beta\text{-}X^{IV}W_8O_{31})_2]^{14-}$ (X = Si, Ge): magnetic, biological, and electrochemical studies, Inorg. Chem. 55 (21) (2016) 10936–10946, https://doi.org/10.1021/acs.inorgchem.6b01458.

[29] Z. Ilyas, H.S. Shah, R. Al-Oweini, U. Kortz, J. Iqbal, Antidiabetic potential of polyoxotungstates: *in vitro* and *in vivo* studies, Metallomics 6 (8) (2014) 1521–1526,

https://doi.org/10.1039/C4MT00106K.
[30] M. Arefian, M. Mirzaei, H. Eshtiagh-Hosseini, A. Frontera, A survey of the different roles of polyoxometalates in their interaction with amino acids, peptides and proteins, Dalton Trans. 46 (21) (2017) 6812–6829, https://doi.org/10.1039/C7DT00894E.
[31] Y. Qi, Y. Xiang, J. Wang, Y. Qi, J. Li, J. Niu, J. Zhong, Inhibition of hepatitis C virus infection by polyoxometalates, Antivir. Res. 100 (2) (2013) 392–398, https://doi.org/10.1016/j.antiviral.2013.08.025.
[32] J. Geng, M. Li, J. Ren, E. Wang, X. Qu, Polyoxometalates as inhibitors of the aggregation of amyloid β peptides associated with Alzheimer's disease, Angew. Chem. Int. Ed. 50 (18) (2011) 4184–4188, https://doi.org/10.1002/ange.201007067.
[33] Z. Han, E. Wang, G. Luan, Y. Li, H. Zhang, Y. Duan, C. Hua, N. Hu, Synthesis, properties and structural characterization of an intermolecular photosensitive complex: $(HGly\text{-}Gly)_3PMo_{12}O_{40}\cdot 4H_2O$, J. Mater. Chem. 12 (4) (2002) 1169–1173, https://doi.org/10.1039/B107225K.
[34] T. Mazari, C.R. Marchal, S. Hocine, N. Salhi, C. Rabia, Oxidation of propane over substituted Keggin phosphomolybdate salts, J. Energy Chem. 3 (18) (2009) 319–324, https://doi.org/10.1016/S1003-9953(08)60111-5.
[35] F. Iftikhar, F. Yoqoob, N. Tabassum, M.S. Jan, A. Sadiq, S. Tahir, T. Batool, B. Niaz, F.L. Ansari, M.I. Choudhary, U. Rashid, Design, synthesis, *in-vitro* thymidine phosphorylase inhibition, *in-vivo* antiangiogenic and in-silico studies of C-6 substituted dihydropyrimidines, Bioorg. Chem. 80 (2018) 99–111, https://doi.org/10.1016/j.bioorg.2018.05.026.
[36] R. Xing, F. Wang, L. Dong, A.P. Zheng, L. Wang, W.J. Su, T. Lin, Inhibitory effects of $Na_7PMo_{11}CuO_{40}$ on mushroom tyrosinase and melanin formation and its antimicrobial activities, Food Chem. 197 (2016) 205–211, https://doi.org/10.1016/j.foodchem.2015.10.119.
[37] M. Ali, K.M. Khan, U. Salar, M. Ashraf, M. Taha, A. Wadood, S. Hamid, M. Riaz, B. Ali, S. Shamim, F. Ali, S. Perveen, Synthesis, *in vitro* α-glucosidase inhibitory activity, and *in silico* study of (E)-thiosemicarbazones and (E)-2-(2-(arylmethylene) hydrazinyl)-4- arylthiazole derivatives, Mol. Divers. (2018) 1–21, https://doi.org/10.1007/s11030-018-9835-2.
[38] C. Scholz, S. Knorr, K. Hamacher, B. Schmidt, DOCKTITE-a highly versatile step-by-step workflow for covalent docking and virtual screening in the molecular operating environment, J. Chem. Inf. Model. 55 (2) (2015) 398–406, https://doi.org/10.1021/ci500681r.
[39] M.S. Islam, A. Barakat, A.M. Al-Majid, M. Ali, S. Yousuf, M.I. Choudhary, R. Khalil, Ul-Haq, Z., Catalytic asymmetric synthesis of indole derivatives as novel α-glucosidase inhibitors *in vitro*, Bioorg. Chem. 79 (2018) 350–354, https://doi.org/10.1016/j.bioorg.2018.05.004.
[40] M. Taha, N.H. Ismail, S. Imran, A. Wadood, M. Ali, F. Rahim, A.A. Khan, M. Riaz, Novel thiosemicarbazide-oxadiazole hybrids as unprecedented inhibitors of *yeast* α-glucosidase and in silico binding analysis, RSC Adv. 6 (40) (2016) 33733–33742, https://doi.org/10.1039/C5RA28012E.
[41] M. Mohammadi-Khanaposhtani, S. Rezaei, R. Khalifeh, S. Imanparast, M.A. Faramarzi, S. Bahadorikhalili, M. Safavi, F. Bandarian, E.N. Esfahani, M. Mahdavi, B. Larijani, Design, synthesis, docking study, α-glucosidase inhibition, and cytotoxic activities of acridine linked to thioacetamides as novel agents in treatment of type 2 diabetes, Bioorg. Chem. 80 (2018) 288–295, https://doi.org/10.1016/j.bioorg.2018.06.035.
[42] R. Xing, A. Zheng, F. Wang, L. Wang, Y. Yu, A. Jiang, Functionality study of $Na_6PMo_{11}FeO_{40}$ as a mushroom tyrosinase inhibitor, Food Chem. 175 (2015) 292–299, https://doi.org/10.1016/j.foodchem.2014.11.157.
[43] Q. Wu, J. Wang, L. Zhang, A. Hong, J. Ren, Molecular recognition of basic fibroblast growth factor by polyoxometalates, Angew. Chem. Int. Ed. Eng. 44 (26) (2005) 4048–4052, https://doi.org/10.1002/anie.200500108.